arXiv:1108.1278v2 [physics.bio-ph] 15 Feb 2012

Spatio-temporal dynamics of bumblebees foraging under predation risk

Friedrich Lenz,¹ Thomas C. Ings,² Lars Chittka,² Aleksei V. Chechkin,³ and Rainer Klages^{1, *}

¹School of Mathematical Sciences, Queen Mary University of London, Mile End Road, London E1 4NS, UK

²School of Biological and Chemical Sciences, Queen Mary University of London, Mile End Road, London E1 4NS, UK

³Institute for Theoretical Physics, NSC KIPT, ul. Akademicheskaya 1,UA-61108 Kharkov, Ukraine

We analyze 3D flight paths of bumblebees searching for nectar in a laboratory experiment with and without predation risk from artificial spiders. For the flight velocities we find mixed probability distributions reflecting the access to the food sources while the threat posed by the spiders shows up only in the velocity correlations. The bumblebees thus adjust their flight patterns spatially to the environment and temporally to predation risk. Key information on response to environmental changes is contained in temporal correlation functions, as we explain by a simple emergent model.

PACS numbers: 87.10.-e, 87.19.lv, 05.40.Fb

Quantifying foraging behavior of organisms by statistical analysis has raised the question whether biologically relevant search strategies can be identified by mathematical modeling [1-7]. For sparsely, randomly distributed, replenishing food sources, the Lévy flight hypothesis predicts that a random search with jump lengths following a power law minimizes the search time [7-9]. Experimental evidence [10-13]and further theoretical analyses [14, 15] supporting this hypothesis were challenged by refined statistical data analyses [16–19] and more detailed theoretical modeling [6, 20, 21]. A crucial problem is how dispositions of a forager like memory [22] or sensory perception [23], as well as properties of the environment [12, 13, 24–27], can be tested in a statistical foraging analysis [1-3, 5, 7]. Especially for data obtained from foraging experiments in the wild, it is typically not clear to which extent extracted search patterns are determined by forager dispositions, or reflect an adjustment of the dynamics of organisms to the distribution of food sources and the presence of predators [5, 12, 13]. This problem can be addressed by statistically quantifying search behavior in laboratory experiments where foraging conditions are varied in a fully controlled manner [13, 24]. Such an experiment has been performed by Ings and Chittka [28, 29], who studied the foraging behavior of bumblebees with and without different types of artificial spiders mimicking predators.

Here we ask the question whether changes of environmental conditions as performed in the experiment by Ings and Chittka lead to changes in the foraging process. We answer this question by a statistical analysis of the bumblebee flights recorded in this experiment on both spatial and temporal scales. For this purpose, we extract both flight velocity probability distributions and temporal velocity autocorrelation functions from the data. Surprisingly, we find that the crucial quantity to understand changes in the bumblebee dynamics under predation risk is not the velocity distribution but the velocity correlation function, which reveals non-trivial dynamics on different time scales. We reproduce these changes by a simple Langevin equation modeling a repulsive interaction between insect and predator. In order to construct mathematical models reproducing the foraging of organisms that interact with the environment, our results suggest to shift the focus from scale-free

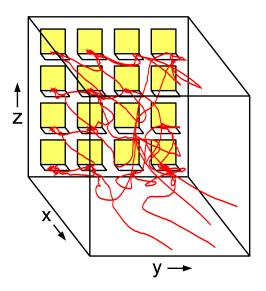


Figure 1. Diagram of the foraging arena together with part of the flight trajectory of a single bumblebee. The bumblebees forage on a grid of artificial flowers on one wall of the box. While being on the landing platforms, the bumblebees have access to food supply. All flowers can be equipped with spider models and trapping mechanisms simulating predation attempts.

approaches [7, 9, 10] to the statistical quantification of spatiotemporal changes in the foraging dynamics.

In the experiment [28] bumblebees (*Bombus terrestris*) were flying in a cubic arena of $\approx 75 \text{ cm}$ side length by foraging on a 4×4 vertical grid of artificial yellow flowers on one wall. The 3D flight trajectories of 30 bumblebees, tested sequentially and individually, were tracked by two high frame rate cameras ($\Delta t = 0.02 \text{ s}$). On the landing platform of each flower, nectar was given to the bumblebees and replenished after consumption. The short trajectory in Fig. 1 shows a typical flight path of a bumblebee foraging in the arena. To analyze differences in the foraging behavior of the bumblebees under threat of predation, artificial spiders were introduced. The experiment was staged into three phases: (1) spider-free foraging, (2) foraging under predation risk and (3) a memory test one day later. Before and directly after stage (2) the

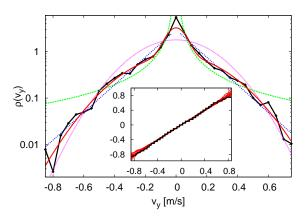


Figure 2. Estimated velocity distributions (main part) and Quantile-Quantile probability plot of a Gaussian mixture as the best fit (inset). Semi-logarithmic plot of the normalized histogram of velocities v_y parallel to the y-axis in Fig. 1 (black crosses) for a single bumblebee in the spider-free stage (1) together with a Gaussian mixture (red line), exponential (blue dotted), power law (green dashed), and Gaussian distribution (violet dotted), fitted via maximum likelihood estimation. The inset shows quantiles of v_y (in m/s) of a single bumblebee against quantiles of an estimated mixture of two Gaussians. An ideal match would yield a straight line. The dashed red lines show 20 surrogate data sets of the same size.

bumblebees were trained to forage in the presence of artificial spiders, which were randomly placed on 25% of the flowers. A spider was emulated by a spider model on the flower and a trapping mechanism which held the bumblebee for two seconds to simulate a predation attempt. In (2) and (3) the spiders models were present but the traps were inactive in order to analyze the influence of previous experience with predation risk on the bumblebees' flight dynamics. To determine whether the detectability of the spiders is an important factor, half of the bumblebees were trained on easily visible (white) spider models and half of them on yellow models, which meant that spiders were camouflaged on the yellow flowers; see Ings and Chittka [28] for further details of the experiment.

Figure 2 shows a typical normalized histogram of the horizontal velocities parallel to the flower wall (cf. y-direction in Fig. 1) for a single bumblebee. The histograms are characterized by a peak at low velocities and vary in the different spatial directions due to asymmetries induced by physical and biological constraints as well as the spatial arrangement of the flowers. Direct fitting of distributions on the histogram and a visual comparison with some assumed distribution was shown to be unreliable [17], as is illustrated by Fig. 2: only the power law and the Gaussian distribution can be ruled out by visual inspection. However, the Gaussian mixture and an exponential function appear to be equally likely. Therefore we use the maximum likelihood method for a number of candidate distributions to obtain the optimal parameters for each candidate and then compare the different distribution types by their weights using the Akaike information criterion [16]. Our candidate distributions are: (a) Exponential: $\rho_{\lambda}(v) = c e^{-\lambda |v|}$, (b) Power law: $\rho_{\mu}(v) = c |v|^{-\mu}$, (c) Normal distribution with

zero mean: $\rho_{\sigma}(v) = N_{\sigma}(v)$, (d) Mixture of two normal distributions: $\rho_{a,\sigma_1,\sigma_2}(v) = aN_{\sigma_1}(v) + (1-a)N_{\sigma_2}(v)$, where $N_{\sigma_i}(v) = \frac{1}{\sqrt{2\pi\sigma_i^2}}e^{-\frac{v^2}{2\sigma_i^2}}$, i = 1, 2, and $0 \le a \le 1$. Details of this analysis are described in the Supplemental Material [34].

For the data sets of all bumblebees and in all stages of the experiment the Akaike weights show that a mixture of two Gaussians is the preferred distribution of the tested candidates (see Table I in the Supplemental Material [34]). However, they do not inform us if the best of the candidates is actually a good model: if all of the candidates are far off the real distribution, the Akaike weights could highlight one of them as the best of the poor fits. As a supplementary qualitative test to which extent the estimated distribution with the largest Akaike weight deviates from the data over the whole range variables, we use Quantile-Quantile (Q-Q) probability plots. The inset of Fig. 2 shows the Q-Q plot of the mixture of two Gaussians against the experimental data of a single bumblebee and 20 surrogate data sets. Each of the surrogate data sets consists of independently identically distributed random numbers drawn from the estimated Gaussian mixture and has the same number of data points as the real data for comparison with statistical fluctuations. The Q-Q plot shows that the deviations of the experimental data from the mixture of two Gaussians is not larger than the expected deviations due to the finite quantity of data.

The Gaussian mixture for the velocities is generated by different flight behavior near a flower versus in open space, which bears some resemblance to intermittent dynamics [6, 7, 25]. This has been verified by splitting the data into flights far from the flower wall vs. flights in the feeding zone. The latter was defined by a cube of side length 9 cm around each flower in which the velocities are determined by approaching a flower and hovering behavior. This separation of different flight phases is thus adapted to accessing the food sources and explains the origin of Gaussian distributions with different variances in both spatial regions. Because of the absence of a sparse distribution of food sources, there was no reason to expect Lévy-type probability distributions [9]. Surprisingly, by comparing the best fits to these distributions for the different stages of the experiment, we could not detect any differences in the velocity distributions between the spider-free stage and the stages where artificial spider models were present, as is shown in Table II of the Supplemental Material [34]. The parameters of the Gaussian mixture vary between individual bumblebees but there is no systematic change due to the presence of predators.

Hence, we examined the velocity autocorrelations for complete flights from flower to flower. The autocorrelations have been computed by averaging over all bumblebees while weighting with the amount of data available for each time interval; see the Supplemental Material for details [34]. Figure 3 shows the velocity autocorrelations in the x- and y-directions for different stages of the experiment. In the x-direction perpendicular to the wall the velocities are always anti-correlated for times around 0.5 s (Fig. 3(a)), which is due to the tendency of the bumblebees to quickly return to the flower wall. However, the flights with long durations between flower visits become more frequent for stages (2) and (3) where the bumblebees were exposed to predation risk compared with stage (1) (inset of Fig. 3(a)). This is also reflected in a small shift of the global minimum in the correlations for stages (2) and (3) away from the origin. The v_x -autocorrelations thus display similar functional forms but with quantitative changes between the different stages. In contrast, for the v_u -autocorrelations the functional forms change profoundly: Parallel to the flower wall the velocities are anti-correlated in the presence of spiders for $0.7 \,\mathrm{s} < \tau < 2.8 \,\mathrm{s}$, while for the spider-free stage the correlations remain positive up to 1.7 s (Fig. 3(b)). The vertical z-direction is similar to the y-direction with a weaker dependence on the presence of predators. As the limited amount of data causes variations in the autocorrelations between individual bumblebees, we resampled the result by leaving the data of each single bumblebee out (jackknifing). The resampling (inset of Fig. 3(b)) confirms that the positive autocorrelations of v_y are not a numerical artifact.

Our statistical analysis of the experimental data has thus revealed that differences in the foraging behavior of bumblebees, triggered by predation risk, show up in changes of the velocity autocorrelation functions only, and not in modifications of the velocity probability distributions. These changes are consistent with a more careful search: When no threat of predators is present, the bumblebees forage more systematically with more or less direct flights from flower to flower, arching away from the flower wall. Under threat the trajectories become longer and the bumblebees change their direction more often in their search for food sources, rejecting flowers with spiders, as is supported by Fig. 3. Further analysis rules out that the main features of the correlation functions are induced by the geometry of the experiment: In Fig. 3(a), all flight time distributions display maxima around $T_f \approx 0.5 \,\mathrm{s}$ suggesting that times below $\simeq 2 \, \mathrm{s}$ are primarily related to flights between flowers. Boundary effects are only evident for flight times that fall within the tail of the distributions. The anti-correlations in the y- and z-directions parallel to the flower wall thus cannot be induced by the walls but are generated by a reversal of directions at flowers under predatory threat. For the x-direction, the return to the flower wall is responsible for the anti-correlation at small delay times, not the opposite wall, which is too far away to have a significant effect. Another interesting aspect is that Ings and Chittka [28] report that bumblebees increase the time they spend inspecting flowers bearing camouflaged spiders compared to conspicuous ones. However, we did not detect any change in velocity distributions or autocorrelations in this case, which suggests that the bumblebees perform longer localized inspection flights without changing their velocities.

In order to understand the changes shown in Fig. 3, we model the dynamics of v_y by the Langevin equation

$$\frac{dv_y}{dt}(t) = -\eta v_y(t) - \frac{\partial U}{\partial y}(y(t)) + \xi(t)$$

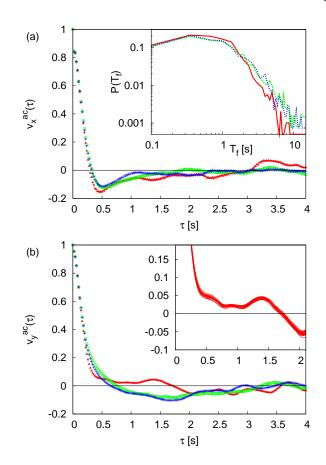


Figure 3. Autocorrelation of the velocities at different experimental stages: without spiders (red triangles), under threat of predation (green circles), and under threat a day after the last encounter with the spiders (blue crosses). (a) In the x-direction perpendicular to the wall the velocities are anti-correlated for small times (≈ 0.5 s) due to short flights from one flower to a nearby flower back at the flower wall. Inset: the distribution of flight times T_f for each stage shows a corresponding maximum for these short jumps. Under threat of predation (dotted) long flights become more frequent. (b) The correlation of v_y parallel to the wall shows the effect of the presence of spiders on the flight behavior of the bumblebees. The inset shows the resampled autocorrelation for the spider-free stage in the region where the correlation differs from the stages with spider models, which confirms that the positive autocorrelations are not a numerical artifact.

where η is a friction coefficient and ξ Gaussian white noise. The potential U mimics an interaction between bumblebee and spider. Specific data analysis shows that this force is repulsive and dominates any hovering behavior in the velocity correlation decay. Computer simulations of the above equation reproduce a change from positive to anti-correlations by increasing the repulsive force. Details are discussed in the Supplemental Material [34]. Note that the correlation decay displayed in Fig. 3 rules out a mathematical modeling in terms of ordinary correlated random walks or Lévy walks, which predict velocity correlations to decay strictly exponentially [7, 26] or algebraically [30, 31], respectively.

We emphasize that the experiment analyzed in this Letter

does not match the conditions of the Lévy flight hypothesis [9]. Lévy flights and Lévy walks predict scale-free probability distributions [7] and generate trivial functional forms for the velocity correlations [30, 31]. Accordingly, experiments testing this hypothesis have focused on probability distributions, not on correlation decay [10–13]. However, our results demonstrate that velocity autocorrelations can contain crucial information for understanding foraging dynamics, here in the form of a highly non-trivial correlation decay emerging from an interaction between forager and predator. Identifying such an emergent property in contrast to adaptive behavior, as we do with our simple model, has been highlighted as a crucial problem in foraging dynamics [13]. In addition, we observe a spatial variation of the velocity distributions. These findings illustrate the presence of different flight modes governing the foraging dynamics on different scales of time and space. Our results thus indicate that taking scale-free distributions as a paradigm beyond the conditions of validity of the Lévy flight hypothesis might be too restrictive an approach in order to capture complex foraging dynamics. A variety of mechanisms may naturally lead to different foraging dynamics on different length and time scales, e.g., individuality of animals [19, 32, 33], an intermittent switching between quasi-ballistic persistent dynamics and localized search modes [6, 18], or quantities over which one has averaged like time of day [13]. As ignoring these mechanisms can lead to spurious power laws [16, 17], it is important to look for the reasons of the occurrence of non-trivial distributions like mixtures, e.g., animals switching between different search modes. These mixtures may not always be optimal distributions for a particular search problem, but they are easy to produce, composable and flexible enough such that differences to some optimal distribution might not be large enough to give rise to evolutionary pressure [4].

In summary, the fundamental question 'What is the mathematically most efficient search strategy of foraging organisms?' has, under specific conditions [21], been answered by the Lévy flight hypothesis [8, 9]. This question is well-posed under precise foraging conditions and has the big advantage that it is amenable to mathematical analysis. However, it does not capture the full complexity of a biological foraging problem [7], which incorporates both the dependence of foraging on 'internal' conditions of a forager (sensory perception [23], memory [22], individuality [19, 32, 33]) as well as 'external' environmental constraints (distribution of food sources [12, 13, 27], day-night cycle [13], predators [28, 29]). Asking about the range of applicability of the Lévy flight hypothesis leads to the over-arching question 'How can we statistically quantify changes in foraging dynamics due to interactions with the environment?', which requires to identify suitable measurable quantities characterizing such changes. This question highlights the need to better understand, and more carefully analyze, the interplay between forager and environment, which will yield crucial information for constructing more general mathematical foraging models.

We thank Holger Kantz for valuable support and Nicholas

W. Watkins as well as Michael F. Shlesinger for helpful comments. Financial support by the EPSRC for a small grant within the framework of the QMUL Bridging The Gap initiative is gratefully acknowledged.

- r.klages@qmul.ac.uk
- [1] G. H. Pyke, H. R. Pulliam, and E. L. Charnov, Q. Rev. Biol., 52, 137 (1977).
- [2] R. S. Schick et al., Ecology Letters, 11, 1338 (2008).
- [3] F. Bartumeus, Oikos, 118, 488 (2009).
- [4] M. G. E. da Luz, A. Grosberg, E. P. Raposo, and G. M. Viswanathan, J. Phys. A: Math. Theor., 42 (2009).
- [5] P. Smouse et al., Phil. Trans. R. Soc. B, 2201 (2010).
- [6] O. Bénichou, C. Loverdo, M. Moreau, and R. Voituriez, Rev. Mod. Phys., 83, 81 (2011).
- G. Viswanathan, M. da Luz, E. Raposo, and H. Stanley, The [7] Physics of Foraging (Cambridge University Press, Cambridge, 2011).
- [8] M. F. Shlesinger and J. Klafter, On Growth and Form, 279 (1985).
- [9] G. M. Viswanathan et al., Nature, 401, 911 (1999).
- [10] G. M. Viswanathan et al., Nature, 381, 413 (1996).
- [11] A. M. Reynolds et al., Ecology, 88, 1955 (2007).
- [12] D. W. Sims et al., Nature, 451, 1098 (2008).
- [13] N. E. Humphries et al., Nature, 465, 1066 (2010).
- [14] M. Lomholt, T. Koren, R. Metzler, and J. Klafter, Proc. Natl. Acad. Sci. USA, 105, 11055 (2008).
- [15] A. M. Reynolds, Behav. Ecol. Sociobiol., 64, 19 (2009).
- [16] A. M. Edwards et al., Nature, 449, 1044 (2007).
- [17] A. M. Edwards, J. Anim. Ecol., 77, 1212 (2008).
- [18] P. Dieterich, R. Klages, R. Preuss, and A. Schwab, Proc. Natl. Acad. Sci. USA, 105, 459 (2008).
- [19] S. Hapca, J. W. Crawford, and I. M. Young, J. R. Soc. Interface, 6, 111 (2009).
- [20] D. W. Sims, D. Righton, and J. W. Pitchford, J. Anim. Ecol., 76, 1365 (2007).
- [21] A. James, J. W. Pitchford, and M. J. Plank, Bull. Math. Biol., 72, 896 (2010).
- [22] J. Burns and J. Thomson, Behavioral Ecology, 17, 48 (2005).
- [23] J. Spaethe, J. Tautz, and L. Chittka, Proc. Natl. Acad. Sci. USA, 98, 3898 (2001).
- [24] F. Bartumeus, F. Peters, S. Pueyo, C. Marrase, and J. Catalan, Proc. Natl. Acad. Sci. USA, 100, 12771 (2003).
- [25] J. M. Morales et al., Ecology, 85, 2436 (2004).
- [26] F. Bartumeus, M. Da Luz, G. Viswanathan, and J. Catalan, Ecology, 86, 3078 (2005).
- [27] E. Kai et al., Proc. Natl. Acad. Sci. USA, 106, 8245 (2009).
- [28] T. C. Ings and L. Chittka, Current Biology, 18, 1520 (2008).
- [29] T. C. Ings and L. Chittka, Proc. R. Soc. B-Biol. Sci., 276, 2031 (2009).
- [30] T. Geisel, J. Nierwetberg, and A. Zacherl, Phys. Rev. Lett., 54, 616 (1985).
- [31] G. Zumofen and J. Klafter, Physica D, 69, 436 (1993).
- [32] S. Petrovskii and A. Morozov, The American Naturalist, 173, 278 (2009).
- [33] C. Hawkes, J. Anim. Ecol., 78, 894 (2009).
- [34] See Supplemental Material at [+++ URL inserted by publisher] for details on the data analysis and for a discussion of the mathematical modeling.

SUPPLEMENTAL MATERIAL

1. Statistical data analysis

To capture bumblebee flights only, we exclude any crawling behavior on the landing platforms by also removing all data within a 1 cm boundary region of each platform. The size of this boundary is based on the size of the bumblebees, which have a height of approximately 1 cm. While smaller cutoffs would not exclude all crawling behavior, the cutoff can be increased robustly within reasonable bounds. We have checked that, e.g. a 2 cm cutoff does not have any influence on any of the analyzed quantities, as the amount of the data which would be excluded in addition is very small. This leaves from 2000 to 15000 data points (average: 6000) per bumblebee for each stage. We select the best model for the velocity distributions by maximum likelihood estimation and Akaike and Bayesian weights for our candidate distributions [16] for $|v| \ge 2.5$ cm/s. Given a set of measured velocities $D = \{v_1, v_2, ..., v_n\}$ and a probability density function $\rho_{\lambda}(v)$, where λ is a vector of k parameters, the log-likelihood of the probability density function for a finite resolution of the data ($\Delta v = 5 \, \mathrm{cm/s}$) simplifies to

$$\ln L(\lambda|D) = \sum_{v_j \in D} \ln P_{\lambda}(v_j) = \sum_{b \in bins} h[b] \ln \int_{min(b)}^{max(b)} \rho_{\lambda}(v) dv$$

where h(b) is the observed frequency in bin b.

For each candidate distribution $\rho_{\lambda_i}^i$, $i \in \{1, 2, 3\}$, we maximize the log-likelihood $\ln L_i$ w.r.t. λ_i locally with a Nelder-Mead algorithm by using a Monte Carlo method to find the global maximum. To find the preference between the different model distributions whose likelihoods L_i are maximized at λ_i^{max} the information criteria are

$$IC_i = -2\ln(L_i(\lambda_i^{max}|D)) + s(n)k_i$$

with s(n) = 2 for the Akaike information criterion and $s(n) = \ln(n)$ for the Bayesian information criterion as a penalty on the number of parameters k_i . The best model, denoted by *, is the one which minimizes the information criterion $IC_* = \min_i (IC_i)$. The Akaike/Bayesian weights then give the preference of each model over the others as a probability

$$w_i = \alpha \mathrm{e}^{-(IC_i - IC_*)/2} \; ,$$

where α normalizes the weights to $\sum_i w_i = 1$.

The choice of the information criterion makes no strong difference for the model selection in this experiment. With the Akaike information criterion the Gaussian mixture is chosen with a weight of over 95% for all bumblebees and all experimental stages. The Bayesian information criterion agrees with the Akaike information criterion on 90% of all data sets. For the other 10% it prefers a single Gaussian or an exponential distribution - these data sets turned out to be those with the least amount of data available.

To compute the autocorrelation function $v^{ac}(\tau)$ of the flight velocities

$$v^{ac}(\tau) = \frac{\langle (v(t) - \mu)(v(t + \tau) - \mu) \rangle}{\sigma^2}$$

we average over all bumblebees and over time in all flights that are complete from starting on one flower to landing on the next. We exclude flights containing gaps and correlation terms, where in-between time t and $t + \tau$ a flower was visited.

Table I. Model weights and estimated parameters. Akaike and Bayesian weights both give preference to the mixture of two Gaussians for v_y for most of the bumblebees. The weights are estimated individually and their mean and standard deviation (in brackets) are shown. The distribution parameters are also estimated individually for each bumblebee in each stage.

Model:	(a) Exponential	(b) Power law	(c) Gaussian	(d) Gaussian Mixture			
Akaike weight	0.00 (0.00)	0.00 (0.00)	0.04 (0.19)	0.96 (0.19)			
Bayesian weight	0.04 (0.18)	0.00 (0.00)	0.08 (0.26)	0.88 (0.30)			
Parameters	λ	μ	σ	a	σ_1	σ_2	
average (bumblebees)	5.61	1.11	0.25	0.67	0.06	0.29	
stddev (bumblebees)	1.07	0.16	0.03	0.13	0.04	0.03	

Table II. Weights and estimated parameters of the Gaussian mixture for the different experimental stages. Weights and parameters are estimated for each bumblebee. Shown are the mean over all individuals and the standard deviation (in brackets). The mixture of two Gaussians is the best fit in all stages. In the parameters of the distribution we observe no significant effect of the threat of predators on the bumblebees.

Stages	Akaike weight	Bayesian weight	a	σ_1	σ_2
(1) Without spiders	0.97 (0.15)	0.93 (0.23)	0.64 (0.11)	0.06 (0.02)	0.29 (0.03)
(2) Under predation risk	0.99 (0.04)	0.90 (0.27)	0.68 (0.13)	0.06 (0.02)	0.29 (0.02)
(3) With risk, 1 day later	0.89 (0.29)	0.80 (0.38)	0.72 (0.16)	0.07 (0.07)	0.30 (0.03)

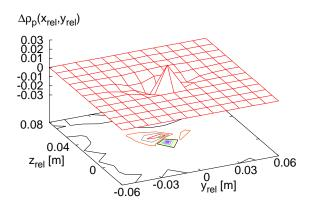


Figure S1. Predator avoidance of bumblebees at flowers, Eq. (1), extracted from the experimental data. Hovering behavior in front of a flower is represented by the positive spike directly at the flower center, while the negative region behind this spike reflects the avoidance in the flights towards a flower.

2. Mathematical modeling of bumblebee foraging

The effect of the presence of a spider on the probability of a bumblebee to fly in front of a flower can be measured by computing the difference between the position densities at stage (1) and (2) as a function of the positions parallel to and near (x < 5 cm) the flower wall,

$$\Delta \rho_p(y_{rel}, z_{rel}) = \rho_p^{(2)}(y_{rel}, z_{rel}) - \rho_p^{(1)}(y_{rel}, z_{rel}) , \quad (1)$$

where the positions (y_{rel}, z_{rel}) are relative to the nearest flower center. This predator avoidance extracted from the experimental data is shown in Fig. S1. Two different types of behavior can be seen: First, there is a small increase in the amount of hovering, i.e. inspection flights near the flower platform when a spider model is present [1, 2], which is consistent with Ref. [3]. However, more important is the local minimum representing the avoidance of flowers infected by spiders. This effect is strongest 3 cm above the dangerous flowers, because the flowers are predominantly approached from above. The avoidance behavior affects not only flights near the flower wall but can still be detected further away from it. Comparing dangerous and safe flowers at stage (2) only confirms that avoidance is the dominant effect for search flights.

The avoidance of spider-infected flowers together with the spatial switching of flight modes discussed in the main part of our Letter can be modeled by the Langevin Equation

$$\frac{d\mathbf{r}}{dt}(t) = \mathbf{v}(t)$$
$$\frac{d\mathbf{v}}{dt}(t) = -\eta \mathbf{v}(t) - \nabla U(\mathbf{r}(t)) + \xi(\mathbf{r}, t) , \qquad (2)$$

where η is a friction coefficient and ξ white Gaussian noise with standard deviation depending on the flight mode as a function of the position, $\xi(\mathbf{r},t) = \chi_{\mathbf{fZ}}(\mathbf{r})\xi_1(t) + (1 - \chi_{\mathbf{fZ}}(\mathbf{r}))\xi_2(t)$. Here $\mathbf{r} = (x, y, z)^{\top}$ is the position of the bumblebee at time t, $\chi_{\mathbf{fZ}}(\mathbf{r})$ is the indicator function of the feeding zone, which is equal to one whenever the bumblebee is in the cube around a flower as defined before, and ξ_i , i = 1, 2 is Gaussian noise with two different variances. The potential U models an interaction between bumblebee and spider in form of a repulsive force exerted by the spider onto the bumblebee, for which we assume that the potential maxima are located near infected flowers.

When the mechanism generating the correlation functions shown in Fig. 3 is not the focus of the investigation, it suffices to consider a reduced version of Eqs. (2) in form of the *effective* Langevin equation

$$\frac{d\mathbf{r}}{dt} = \chi_{\mathbf{f}\mathbf{Z}}(\mathbf{r})\zeta_1(t) + (1 - \chi_{\mathbf{f}\mathbf{Z}}(\mathbf{r}))\zeta_2(t) .$$
(3)

This equation describes the spatially varying hovering and search modes by using noise ζ_i , i = 1, 2., which models the impact of the potential U together with the noise ξ . Further data analysis shows that excluding hovering has no significant impact on the velocity autocorrelations, which are dominated by the search flights. This is in full agreement with Fig. 3, where the time scale for the predator-induced anti-correlation (Fig. 3(b)) is larger than the time scale for flights between neighbouring flowers (Fig. 3(a)). Hence, we model $\zeta_1(t)$ as a vector of Gaussian white noise with the smaller variance σ_1^2 given in Table I which describes the hovering. The search flights from flower to flower are reproduced by the correlated Gaussian noise vector $\zeta_2(t)$ with variance σ_2^2 and the autocorrelations $v_i^{ac}(\tau)$, i = x, y shown in Fig. 3. The advantage of this model is that it is directly based on our data analysis.

We now focus on the different aspect of understanding the biophysical mechanism that generates the anti-correlations of the velocities parallel to y shown in Fig. 3(b). Starting from the full model Eqs. (2), it suffices to select the search mode only by setting $\xi(\mathbf{r}, t) = \xi_2(t)$ thus neglecting any spatial variations of the noise. This yields the Langevin equation

$$\frac{dv_y}{dt}(t) = -\eta v_y(t) - \frac{\partial U}{\partial y}(y(t)) + \xi(t) , \qquad (4)$$

which was already stated in the main part as the main equation. A rough approximation for the repulsive force is provided by a periodic potential with maxima at dangerous flowers,

$$U(\mathbf{r}) = u \cos\left(2\pi \frac{y}{y_0}\right) \,,\tag{5}$$

where y_0 is the mean distance between spiders and u the strength of the repulsion.

We integrated this Langevin equation via an Euler-Maruyama method under variation of u by computing the autocorrelation function v_y^{ac} of the generated data. Figure S2 shows v_y^{ac} by increasing the repulsion strength u. The correlation function changes from positive correlations to anticorrelations in a range of delay times τ comparable to the changes in the correlation function of the experimental data of Fig. 3(b). This qualitatively reproduces our experimental findings from first principles. Note that the oscillations for higher

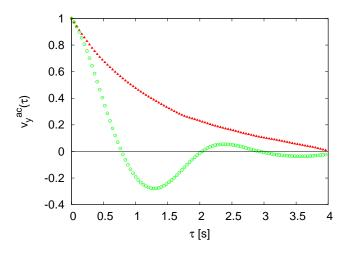


Figure S2. Autocorrelation function of the velocities v_y for the Langevin model Eqs. (4),(5) modeling predation threat by different strengths of a repulsive potential. Shown are results from computer simulations without (u = 0; red triangles, upper line) and with predation threat ($u = 0.5 \text{ m}^2/\text{s}^2$; green circles, lower line). These results should be qualitatively compared with the experimental findings Fig. 3(b).

 τ in Fig. S2 would be suppressed in a higher-dimensional model. The other directions can be treated analogously, e.g., by including an *x*-dependent term in the potential for the attraction of the bumblebees to the flower wall. A stochastic

analysis of Langevin equations with periodic potentials can be found, e.g., in Ref. [4]. The effect of the harmonic potential on the creation of negative velocity correlations can also be calculated analytically [5].

We emphasize that our model Eqs. (4),(5) provides only a qualitative description of the biophysical mechanism generating the change in the correlations of the bumblebee velocities under predation threat. For a quantitative comparison to the experimental data a much more detailed model would be necessary, which needs to include the random positioning of the spiders and the general attractive force exerted by the flowers onto the bumblebees. Modeling the three-dimensional nature of the potential would also be important: Notice, e.g., the local maximum of v_y^{ac} around $\tau \simeq 2.5$ which is an artifact of the one-dimensional modeling of spider avoidance. However, as it is difficult to reliably estimate the parameters of the potential, such a quantitative comparison is beyond the scope of our Letter.

- T. Ings, M. Y. Wang, and L. Chittka, Behavioral Ecology and Sociobiology, 1 (2011).
- [2] T. Yokoi and K. Fujisaki, Naturwissenschaften, 96, 195 (2009).
- [3] T. C. Ings and L. Chittka, Current Biology, 18, 1520 (2008).
- [4] H. Risken, The Fokker-Planck Equation : Methods of Solution and Applications (Springer, Berlin New York, 1989).
- [5] F. Lenz, A. V. Chechkin, T. C. Ings, L. Chittka, and R. Klages, In preparation.